NANO LETTERS

pubs.acs.org/NanoLett

Letter

Intrinsic Formamidinium Tin Iodide Nanocrystals by Suppressing the Sn(IV) Impurities

Dmitry N. Dirin,* Anna Vivani, Marios Zacharias, Taras V. Sekh, Ihor Cherniukh, Sergii Yakunin, Federica Bertolotti, Marcel Aebli, Richard D. Schaller, Alexander Wieczorek, Sebastian Siol, Claudia Cancellieri, Lars P. H. Jeurgens, Norberto Masciocchi, Antonietta Guagliardi, Laurent Pedesseau, Jacky Even, Maksym V. Kovalenko, and Maryna I. Bodnarchuk

Cite This: *Nano Lett.* 2023, 23, 1914−1923

Read Online

ACCESS | Metrics & More | Article Recommendations | Supporting Information

ABSTRACT: The long search for nontoxic alternatives to lead halide perovskites (LHPs) has shown that some compelling properties of LHPs, such as low effective masses of carriers, can only be attained in their closest Sn(II) and Ge(II) analogues, despite their tendency toward oxidation. Judicious choice of chemistry allowed formamidinium tin iodide ($FASnI_3$) to reach a power conversion efficiency of 14.81% in photovoltaic devices. This progress motivated us to develop a synthesis of colloidal $FASnI_3$ NCs with a concentration of Sn(IV) reduced to an insignificant level and to probe their intrinsic structural and optical properties. Intrinsic $FASnI_3$ NCs exhibit unusually low absorption coefficients of 4×10^3 cm^{-1} at the first excitonic transition, a 190 meV increase of the band gap as compared to the bulk material, and a lack of excitonic resonances. These features are attributed to a highly disordered lattice, distinct from the bulk $FASnI_3$ as supported by structural characterizations and first-principles calculations.

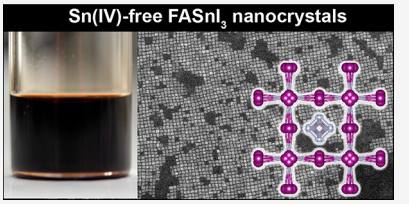

KEYWORDS: *halide perovskite, lead-free, nanocrystals*

In a decade since the landmark works of the Snaith and Grätzel groups,[1,2] lead halide perovskites (LHPs) have paved their way aside from photovoltaics toward many eminently different applications ranging from backlit displays and light-emitting diodes to hard radiation and neutron detection.[3−15] Such a broad utility of LHPs is rooted in a rare combination of their properties, including low density of carrier trap states (10^9−10^{10} cm^{-3}) despite a large density of point defects,[5,16,17] long electron−hole diffusion lengths (2−175 μm),[5,18,19] high carrier mobilities (2.5−1000 cm^2 V^{-1} s^{-1}),[5,17,20−22] long charge carrier lifetimes (0.08−450 μs),[5,18−21,23] small carrier effective masses (0.069−0.25 m_0),[24] and high optical absorption coefficients at the absorption edge ($2-7 \times 10^4$ cm^{-1}).[17] Although LHP-based devices may meet RoHS compliancy in some cases,[25,26] the anticipated scale of the LHP market calls for lead-free alternatives.[27]

Compelling electronic characteristics of LHPs largely arise from the pronounced tolerance to intrinsic defects[28,29] and lattice softness allowing large polarons and efficient screening of the carriers.[30−33] Tin(II)- and germanium(II)-based AMX_3 halide perovskites [A = Cs, formamidinium (FA), or methylammonium (MA)] have always been envisioned as the closest alternatives to LHPs. The metal−halide−metal (M−X−M) angle of about 180° ensures the highest σ overlap of the orbitals and the efficient dispersion of the resulting electronic bands. Tilting the octahedra or alternating cations in other halide perovskitoids reduces orbital overlap, opens the band gap, and leads to heavier carriers.[34,35] Metal halides with edge- or face-sharing octahedra, or even with fully isolated ones (0D-halides), exhibit properties that are notably different from the prototypic LHPs. Although these properties are promising for some applications,[36−47] such materials are unlikely to deliver the photovoltaic performance or narrow-band excitonic luminescence similar to LHPs.

The main factor limiting the performance of Sn and Ge halide perovskites is their low stability toward oxidation, which by a number of pathways can lead to degenerate p-type conductivity.[48] Nevertheless, considerable progress has been achieved in $FASnI_3$-based photovoltaics over the past seven years with a 7-fold increase of the power conversion efficiency (PCE), with a benchmark now of 14.81% (Figure S1).[49,50] Synthetic approaches can be grouped as follows:

(i) reduction of the present Sn(IV) impurities by comproportionation with metallic Sn(0)[51,52]

(ii) altering the lattice of $FASnI_3$ by doping with bifunctional organic cations capable of pinning Sn vacancies (so-called "hollow" structures)[53−58]

Received: December 21, 2022
Revised: February 16, 2023
Published: February 28, 2023

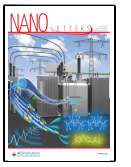

https://doi.org/10.1021/acs.nanolett.2c04927
Nano Lett. 2023, 23, 1914−1923

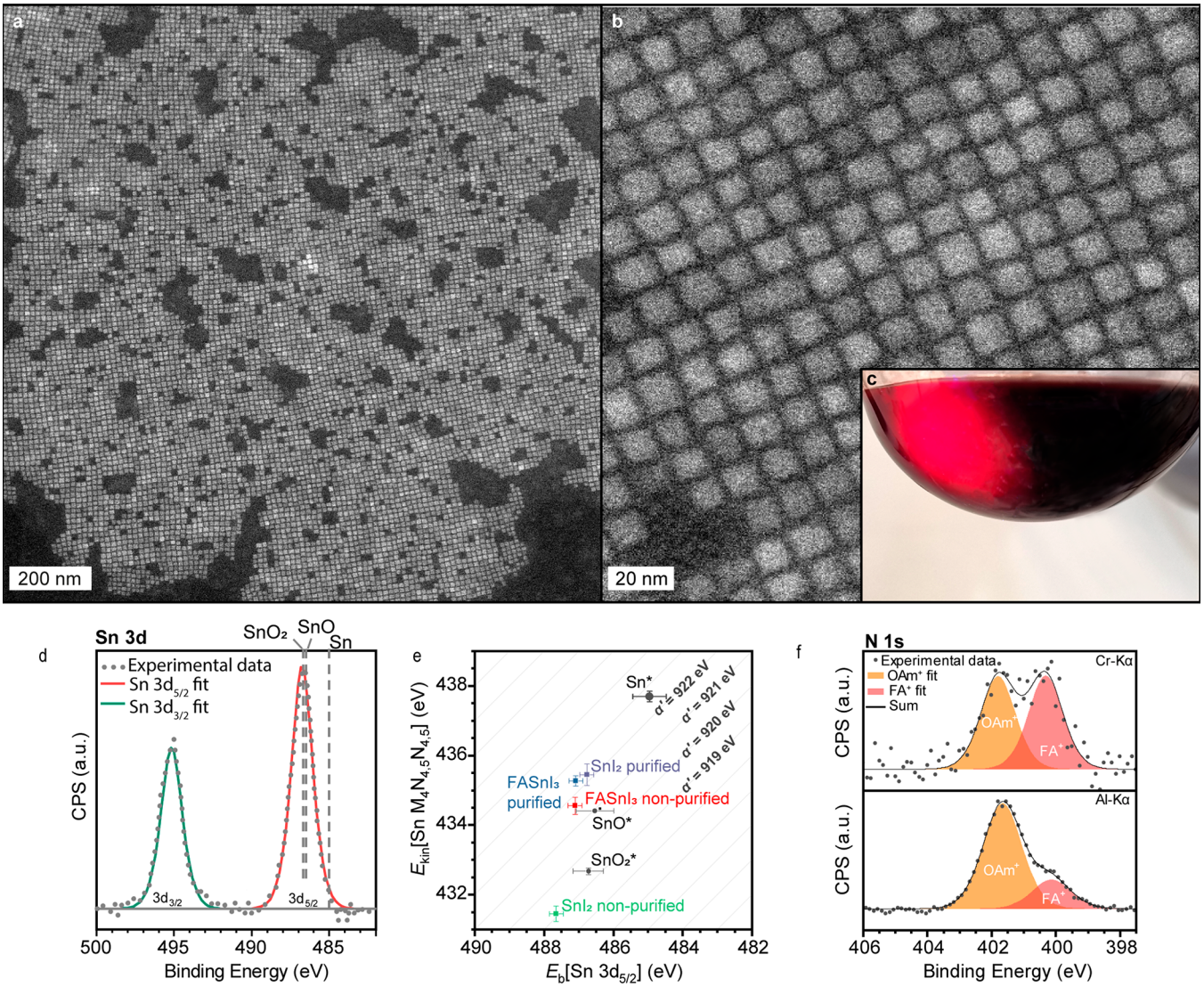

Figure 1. (a, b) DF STEM images of representative $FASnI_3$ NCs. (c) Visual appearance of the crude solution of $FASnI_3$ NCs. (d) XPS Sn 3d spectra of $FASnI_3$ NCs synthesized from purified SnI_2 with corresponding fits and reference peaks for Sn, SnO, and SnO_2 extracted from the NIST database.[60] (e) Wagner plot illustrating modified Auger parameters of Sn in $FASnI_3$ NCs made from purified and nonpurified SnI_2 with the respective references for Sn, SnI_2, SnO, and SnO_2. (f) HAXPES N 1s spectra made with hard (Cr Kα) and soft (Al Kα) X-ray sources.

(iii) passivation of $FASnI_3$ surface with bulky organic cations[59]

In contrast, the synthesis of tin halide perovskite nanocrystals (NCs) remains scarce in the literature and is mainly limited to $CsSnX_3$ or mixed $APb_ySn_{1-y}X_3$ compositions.[61−69] L. Dai et al. have recently reported the protocol allowing the synthesis of $FASnI_3$ NCs with good morphological quality.[70] However, their work focuses on the hot-carrier relaxation processes in $FASnI_3$ NCs and does not discuss the effect of the present impurities on the optical properties of NCs, which we find to be crucial.

We thus sought to develop a colloidal synthesis of $FASnI_3$ NCs with high morphological quality and purity and study their intrinsic optical properties and structure, as reported herein. We devote special care to the purity of all of the involved precursors to exclude possible doping during the synthesis. We show that pure $FASnI_3$ NCs exhibit a disorder of the I-sites that reduces the Sn−I−Sn angle to 167° and opens the band gap by ∼190 meV. Our findings are supported by ab initio calculations for the average cubic structure of $FASnI_3$ showing that the octahedra exhibit a significant tilting that profoundly affects the electronic structure. Such distortion also allows for unusually pronounced photoinduced states. Based on these findings, we propose an additional pathway for tuning the optical properties of $FASnI_3$ NCs via altering their lattice with bifunctional organic cations.

In the footstep of our earlier reports on the synthesis of $FAPbI_3$ NCs, the first edition of $FASnI_3$ NCs involved 1-octadecene (ODE) as a solvent (Figure S2). Briefly, oleylamine (OAm), oleic acid (OA), and formamidinium oleate are sequentially injected into a hot SnI_2 solution in trioctylphosphine (TOP) and ODE. However, we have found two rarely considered important synthetic parameters to be crucial for the synthesis of Sn(IV)-free $FASnI_3$ NCs (see Supporting Information Note S1 for details). First, all tested commercially available sources of SnI_2 are of >99% metal basis purity but contain significant amounts of SnO, SnO_2, and SnI_4 that notably affect the synthesis. Therefore, we have developed a two-step purification procedure that results in SnI_2 with an

https://doi.org/10.1021/acs.nanolett.2c04927
Nano Lett. 2023, 23, 1914−1923

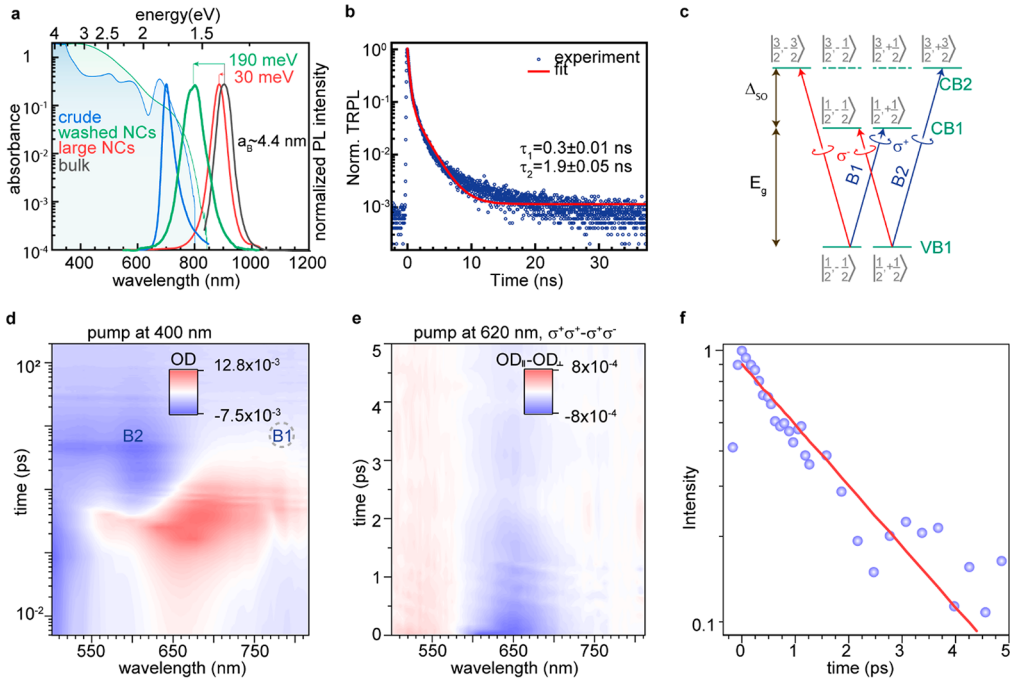

Figure 2. (a) Absorption and PL spectra of $FASnI_3$ NCs; PL spectra of bulk $FASnI_3$ and 200 nm large nanocrystals are shown for comparison. (b) Time-resolved PL spectrum of $FASnI_3$ NCs in solution. (c) Optical selection rules in $FASnI_3$ and corresponding absorption transitions; the spin-polarized states are labeled using $|J, m_J\rangle$. The solid and dashed lines of the $J = 3/2$ states represent heavy and light electrons correspondingly. (d) Pseudocolor 2D plot for room temperature pump−probe TA spectroscopy of colloidal $FASnI_3$ NCs pumped at 400 nm. (e) Net spin pseudocolor 2D plot obtained as a difference between co- and cross-polarized TA spectra pumped at 620 nm. (f) Experimental (blue dots) net spin kinetics with 650 nm probe photons and single-exponent fit (red line).

insignificant amount of Sn(IV) species, as evidenced by X-ray photoelectron spectroscopy (XPS) and X-ray diffraction (XRD). Second, reactions performed at 80 °C in ODE nearly instantly lead to the oxidation of iodide anions to polyiodide ones, apparent from their characteristic red-brown color. Note that photoluminescence (PL) spectra of NCs synthesized in ODE do not correlate with their size, and the PL maximum fluctuates in a broad range from 700 to 850 nm (Figure S3). Therefore, we opt for a synthesis in aromatic solvents (toluene, mesitylene, or Dowtherm A) that proceeds without color change until formamidinium oleate solution is injected and NCs start to grow (Figures S4 and S5).

The optimized synthesis proceeds by solubilizing SnI_2 in Dowtherm A in the presence of oleylamine and TOP, followed by the hot injection of formamidinium oleate dissolved in Dowtherm A (see the SI for the details). The stability of as-prepared NCs is sufficient to wash them by precipitation with acetonitrile, if washing is performed air-free. This protocol allows the removal of all byproducts and impurities of layered perovskites with PL around 700 nm, which is always present in the crude solution (Figures 1a−c).

XPS combined with inert-gas transfer was used to collect the Sn 3d core level spectra.[71] The acquired spectra for Sn $3d_{5/2}$ and $3d_{3/2}$ do not show apparent asymmetry and can be well-fitted with a single component, indicating Sn is mainly present in one oxidation state (Figure 1d). $FASnI_3$ samples made from purified and nonpurified SnI_2 showed great similarity (Figure S6). However, due to the high proximity of peaks corresponding to Sn^{2+} and Sn^{4+} and inaccuracies related to the referencing of the binding energy scale as well as charging effects, the spectrum analysis can sometimes be ambiguous, leading to possibly wrong assumptions about the oxidation state. This is especially the case with low Sn^{2+} or Sn^{4+} contents. The modified Auger parameter, α' (AP),[72] allows one to cancel out shifts related to charging and band bending effects and was shown to be useful for resolving the oxidation state and chemical environment of Sn in perovskite-type structures, including polycrystalline $FASnI_3$ films.[71] The value of α' corresponds to the sum of the binding energy (BE) of the Sn $3d^5/_2$ photoelectron line and the kinetic energy (KE) of the corresponding Sn $M_4N_{4,5}N_{4,5}$ Auger line. Any shift in α' can be directly related to a change in the local electronic polarizability,[72] which is extremely sensitive to changes in the local chemical state of the atom in the compound.[73,74] Shifts in α' can be visualized in a so-called chemical-state (or Wagner) plot, where constant α' values lie on diagonal lines (Figure 1e). Strikingly, the α' value for nonpurified SnI_2 (919.1 eV) is highly similar to that reported for SnO_2, indicating its presence and potentially that of other Sn(IV) compounds on the powder surface. The purified SnI_2, in contrast, exhibits a higher α' value (922.2 eV), similar to other Sn(II) compounds. Likewise, the α' values of the $FASnI_3$ NC films made from purified and nonpurified SnI_2 significantly differ (922.3 eV vs 921.6 eV), with the first value matching precisely the one reported for polycrystalline $FASnI_3$ films.[71] These data demonstrate the enhanced sensitivity of the AP analysis for detecting minuscule differences in the local chemical state of Sn. In agreement with XPS data, we have not observed any signs of the oxidized FA_2SnI_6 form in ^{119}Sn solid-state NMR, which is expected at −4818 ppm.[75] We also did not observe the effect of a number of reducing agents on the optical properties of $FASnI_3$ NCs, as summarized in Supporting Information Note S2. These findings suggest that the amount of Sn(IV) impurities in the synthesized $FASnI_3$ NCs is

https://doi.org/10.1021/acs.nanolett.2c04927
Nano Lett. 2023, 23, 1914−1923

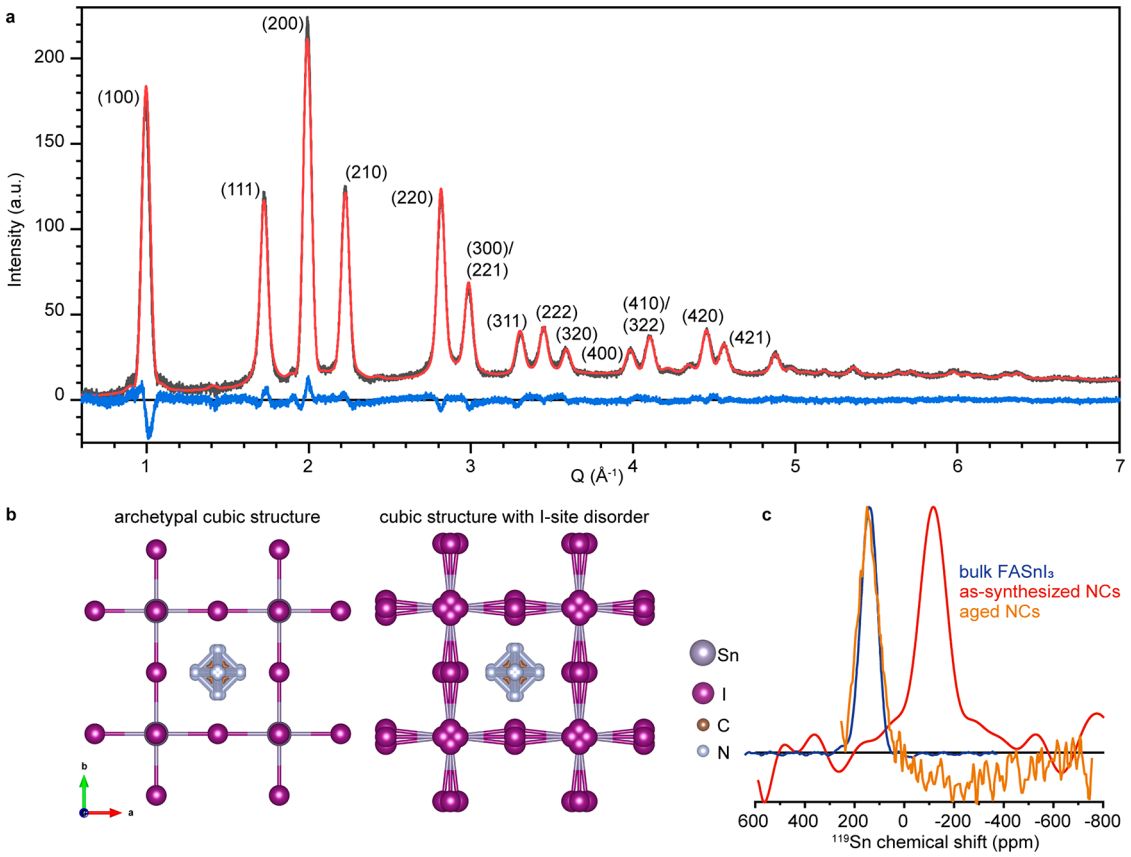

Figure 3. (a) Synchrotron WAXTS data (black curve) collected on colloidal solution of $FASnI_3$ NCs plotted with the solvent signal subtracted, DSE simulation (red trace), and difference profile (blue curve) using the NC disordered cubic ($Pm\bar{3}m$ space group) model including (b) schematic of iodide displacement. In panel b, we also include the inorganic network with iodide disorder as calculated for DFT. (c) Solid-state ^{119}Sn NMR spectra for bulk $FASnI_3$, colloidal, and aged $FASnI_3$ NCs.

insignificant and should not affect the optical properties of the obtained NCs.

The core region of the $FASnI_3$ NCs can be more effectively probed by hard X-ray photoelectron spectroscopy (HAXPES) analysis using a hard Cr Kα X-ray source, resulting in an approximate increase of the information depth by a factor of 3.[76] This comparison helps us to study the distribution of N in the NC core and on the surface in the form of formamidinium (N_{FA}^+) and oleylammonium (N_{OAm}^+), respectively (Figure 1f). HAXPES reveals that the total N_{OAm}^+/N_{FA}^+ ratio (1:1) is lowered compared to that of the XPS analysis (3.6:1), which probes the surface of NCs preferentially. This finding indicates that NCs in solution have a significant amount of unbound OAmI ligands, in agreement with the analogous $CsPbBr_3$ NCs and ICP-MS data showing a strong excess of I over Sn.[77]

Pure colloidal $FASnI_3$ NCs exhibit absorption edge and PL in the range 770−830 nm with PL quantum yield (QY) of 0.1%. (Figure 2a). Time-resolved emission spectra (TRES) are found to be wavelength-independent, confirming the uniformity of the NCs (Figures 2b, Figure S7). PL decay is biexponential with 0.3 ns (90%) and 1.9 ns (10%) lifetimes, in agreement with reported values for bulk $FASnI_3$.[78] The excitonic absorption peak of pure $FASnI_3$ NCs is unresolved, similar to the previously reported spectra of other tin halide perovskite NCs.[62,65] We note that the absorption tail lasting to ~800 nm belongs to NCs and not to the scattering, as ensured by filtering the solution through a 0.2 μm PTFE filter and evidenced by PL upon excitation at 635 nm (Figure S8).

Absorption edge and PL of the synthesized $FASnI_3$ NCs are notably (by 190 meV) shifted from the band gap of bulk $FASnI_3$ (Figure 2a). Although the increase of the band gap is expected for colloidal semiconductor NCs, such a big shift can hardly be explained solely by quantum confinement. For example, the confinement energy in $FAPbI_3$ and $CsPbI_3$ NCs of similar sizes is 89−93 meV.[17,79,80] These NCs are about 10 nm large, whereas the exciton Bohr radius in $FASnI_3$ should be 3.5−4.4 nm, depending on the set of effective masses reported for bulk material,[81,82] indicating that these NCs should be in a weak confinement regime.

Absorption spectra of the pure $FASnI_3$ NCs do not exhibit resolved excitonic transitions despite the narrow size dispersion (8−12%). Furthermore, these NCs exhibit rather low intrinsic absorption of about $4 \pm 1.7 \times 10^3$ cm^{-1} (determined 100 meV above the band gap by the ICP-MS with a combination of acidic and basic digestions for Sn and I, respectively; see Supporting Information Note S3 for details). That is about 4 times lower than the absorption coefficient reported for bulk $FASnI_3$.[83]

Figure 2d shows spectrally resolved transient absorption (TA) data of $FASnI_3$ NCs pumped at 400 nm, well above the band gap. This spectral map reveals a pronounced bleach around 600, ascribed to the VB1-CB2 transition (Figure 2c, see Supporting Information Note S4 for details).[84,85] The net spin relaxation kinetics, evaluated as the difference between co- and cross-polarized TA signals, is fitted using a single-exponential decay and yields a lifetime of 2 ps, on par with the one of LHP

https://doi.org/10.1021/acs.nanolett.2c04927
Nano Lett. 2023, 23, 1914−1923

NCs (~1−3 ps), which is much shorter than in the case of $CsSnBr_3$ NCs (Figures 2e,f).[85]

In addition to the expected bleaches, Figure 5d reveals a pronounced photoinduced absorption (PIA) band below the B2 bleach. Depending on the experimental conditions, this PIA band occurs on different time scales and at slightly different energies (Figure S9). In the case of resonance pumping, the PIA band is polarization-sensitive, appears at ~0.2 ps, has a maximum at 703 nm, correlates with depopulation of B2, and can be explained as a biexciton shift.[76,85] In the case of pumping at 400 nm, in contrast, PIA appears before the thermalization of carriers to the B2 state, has a maximum around 670 nm, and is also significantly more intense. This type of PIA is nearly absent with resonance pumping. We suggest that this PIA can arise due to the additional photoinduced states created upon lattice distortion induced by hot carriers. Fast PIA to these states becomes possible until the hot carrier is thermalized, and lattice distortion is released. Note that such strong PIA was not observed for $CsPbX_3$.[76] In contrast, electron localization has been recently predicted to be energetically favorable in many tin halide perovskites, with bipolaronic states being the most stable form of self-trapped electrons.[86]

We hypothesized that the unusually large band gap, distinct PIA, as well as weak and unresolved absorption transitions in $FASnI_3$ NCs may be related to the reduced lattice symmetry, as evidenced below by wide-angle X-ray total scattering (WAXTS) and solid-state ^{119}Sn NMR data.

$FASnI_3$ NCs exhibit a cubic crystal structure and $Pm\bar{3}m$ space group symmetry (model parameters are reported in Table S1), as recently reported for $FASnI_3$ bulk crystal (Figure 3a).[87,88] Results from both Rietveld refinement[89] and the Debye scattering equation (DSE)-based method[90] agree on a disordered cubic model, where each iodine is replaced by four equivalent ions, offset by 0.36 Å from the original site and lying on a plane perpendicular to the direction of the Sn−Sn axis, each one with a fractional site occupancy factor (sof) of 0.25 (Figure 3b). Such a small local distortion makes the Sn−I−Sn angle bent (by about 13°), while the $Pm\bar{3}m$ cubic symmetry is retained. We verify this picture using density functional theory (DFT) calculations on the average cubic but disordered structure of $FASnI_3$ that yield an average Sn−I−Sn bending of 10° (see computational details in the SI). The presence of this structural disorder is also suggested by the very large isotropic Debye−Waller factors (B) of iodide ions (B(I) > 6 Å^2). Improved modeling of WAXTS data is achieved by splitting the iodide positions, which led to a better match of peak intensities (as detailed in the SI) and reduced B(I) values of 2.8 Å^2. The same model has already been used to represent the structural disorder in $FAPbI_3$ and $FAPbBr_3$ NCs.[79,91] Remarkably, although large atomic displacement parameters of iodine ions (6.3 Å^2) are reported for bulk $FASnI_3$,[87] there was no indication of iodide displacement, while the archetypal cubic structure was favored (Table S2). Despite the considerably high B(Sn) factors (>4 Å^2), WAXTS data for these NCs do not support the local disorder previously reported for bulk samples where Sn is off-centered along the [111] crystallographic direction[92] (not observed in single crystal XRD data of ref 87; see Table S2).

Analogously to WAXTS data, ^{119}Sn solid-state NMR indicates that the lattice symmetry of $FASnI_3$ NCs might be reduced compared to bulk $FASnI_3$: the chemical shift of $FASnI_3$ NCs (−116 ppm) is significantly lower compared to bulk $FASnI_3$ (140 ppm, Figure 3c). Note that, after aging and merging of NCs, the ^{119}Sn chemical shift (144 ppm) coincides with the bulk material, indicating that the signal at −120 ppm is a signature of individual NCs that are not degraded.

Although the time-averaged structure of $FASnI_3$ NCs is cubic, the observed type of disorder can increase the band gap. DFT calculations of the electron spectral function of the disordered cubic $FASnI_3$ (color map) and the band structure of the archetypal cubic $FASnI_3$ (black dots) show that the electronic structure is modified significantly upon allowing the system to accommodate local distortions (Figure 4). In

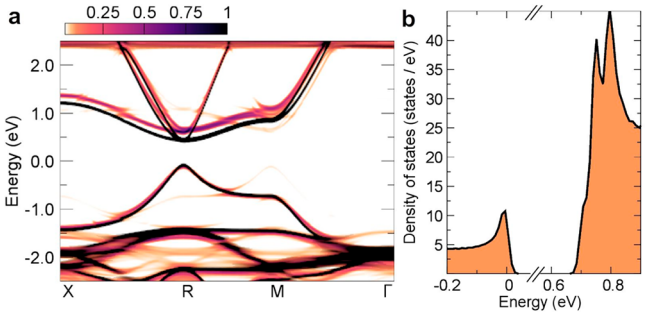

Figure 4. (a) Momentum-resolved electron spectral function and (b) density of states of $FASnI_3$ calculated using the disordered structure in a 2 × 2 × 2 supercell and the band structure unfolding technique.[93] Black lines in panel a represent the electron band structure calculated using the archetypal cubic $FASnI_3$ structure at high-symmetry positions but with the FA molecules in orientations as calculated for the disordered structure.

particular, the band gap increases by ~223 meV due to the reduced Sn−I−Sn angle. This phenomenon is well-known for metal halide perovskite-like compounds.[94] The DOS around the band edges is consistent with the parabolic band approximation varying with the square root of energy. The peak structures in the conduction band reflect the nearly triply degenerate conduction band minimum at the R high symmetry point. Despite the presence of local distortions, the degeneracy should be maintained since the network reflects, on average, a high-symmetry structure. The DFT calculations also reveal the smearing of the electronic structure, which accounts for the absence of excitonic resonances in the absorption spectrum. Moreover, this smearing induces a difference between the Tauc plots for the "direct" or "indirect band model" (see Figure S10 and discussion therein), while still considering zero-phonon optical transition. These simulations show that the highly disordered average cubic lattice of $FASnI_3$ may significantly depart from the standard picture of a perfectly ordered direct-band-gap semiconductor when optoelectronic properties are considered.

The observed lattice disorder and PIA hint that intrinsic $FASnI_3$ NCs are unlikely to exhibit optical properties resembling those of lead halide perovskite NCs. One way to reduce the remarkable, but in this case undesired, smearing of the electronic structure is to alter the lattice via mild doping. This motivated us to explore the possibility of tuning the optical properties of $FASnI_3$ NCs by doping them with small A-site or bifunctional cations (Figure 5, Supporting Information Note S5). Indeed, doping with Cs or ethylenediammonium (up to 5%) leads to the onset of a slightly resolved absorption feature around 700 nm, which is absent in undoped $FASnI_3$ NCs and smears away at higher levels of doping

https://doi.org/10.1021/acs.nanolett.2c04927
Nano Lett. 2023, 23, 1914−1923

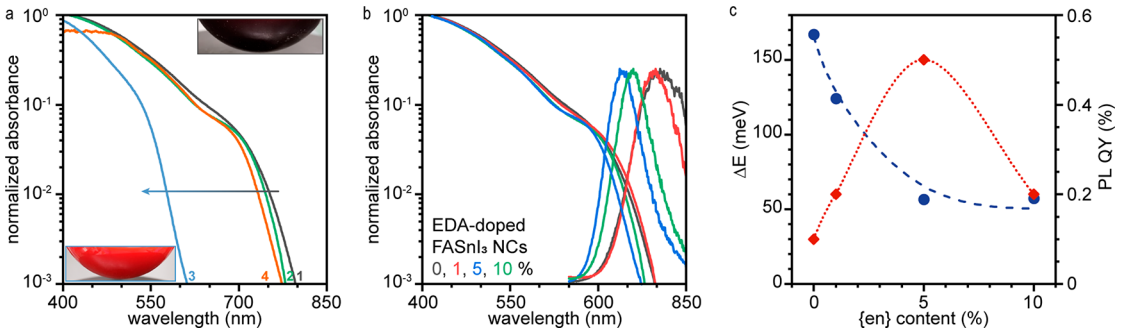

Figure 5. (a) Absorption spectra of undoped (1) colloidal $FASnI_3$ NCs and NCs doped with hydroxyethylammonium (2), ethylenediammonium (3), and Cs (4). (b) Absorption and PL spectra of $FASnI_3$ NCs doped with various amounts of ethylenediammonium. (c) Energy gap (blue) between PL maxima and absorption edges and PL QY (red) as a function of ethylenediammonium loading.

(Figure 5b). This trend coincides with a PL peak shift, notable narrowing, and PL QY dependence on the doping level (Figure 5c). The energy gap between the absorption band edge and PL peak position quickly decreases by 3 times (Figure 5c). Altogether, this indicates that doping may be the right strategy to overcome the observed disorder-induced smearing of the optoelectronic properties in the $FASnI_3$ NCs.

In conclusion, we have developed a colloidal synthesis of monodisperse and Sn(IV)-free $FASnI_3$ NCs, which allowed us to probe their intrinsic optical properties. We show that 10 nm large pure colloidal $FASnI_3$ NCs exhibit an unusually large band gap, which cannot be explained solely by quantum confinement and is instead attributed to the distortion of the lattice through the split of I-sites. Such a split causes a reduction in the symmetry and bending of the Sn−I−Sn bond, reducing the overlap of Sn and I 5p orbitals. Pure $FASnI_3$ NCs also exhibit a nearly featureless absorption spectrum with an absorption coefficient of only $4 \pm 1.7 \times 10^3$ cm^{-1} near the band gap, which might be caused by the disorder-induced smearing of the electronic structure. We also show that doping $FASnI_3$ NCs with bifunctional organic cations, such as ethylenediammonium, might be an efficient way to tune the optical properties of these NCs.

■ ASSOCIATED CONTENT

Supporting Information

The Supporting Information is available free of charge at https://pubs.acs.org/doi/10.1021/acs.nanolett.2c04927.

Synthesis details; characterization techniques; WAXTS analysis; and additional notes and figures including PCE evolution, TEM images, size histograms, PL spectra, PL peak maxima, XPS spectra, TRES, photoluminescence spectra, and PIA results (PDF)

■ AUTHOR INFORMATION

Corresponding Author

Dmitry N. Dirin − *Institute of Inorganic Chemistry, Department of Chemistry and Applied Biosciences, ETH Zürich, CH-8093 Zürich, Switzerland; Empa−Swiss Federal Laboratories for Materials Science and Technology, CH-8600 Dübendorf, Switzerland;* orcid.org/0000-0002-5187-4555; Email: ddirin@ethz.ch

Authors

Anna Vivani − *Dipartimento di Scienza e Alta Tecnologia & To.Sca.Lab, Università dell'Insubria, 22100 Como, Italy*

Marios Zacharias − *Univ Rennes, INSA Rennes, CNRS, Institut FOTON, Rennes F-35000, France*

Taras V. Sekh − *Institute of Inorganic Chemistry, Department of Chemistry and Applied Biosciences, ETH Zürich, CH-8093 Zürich, Switzerland; Empa−Swiss Federal Laboratories for Materials Science and Technology, CH-8600 Dübendorf, Switzerland*

Ihor Cherniukh − *Institute of Inorganic Chemistry, Department of Chemistry and Applied Biosciences, ETH Zürich, CH-8093 Zürich, Switzerland; Empa−Swiss Federal Laboratories for Materials Science and Technology, CH-8600 Dübendorf, Switzerland*

Sergii Yakunin − *Institute of Inorganic Chemistry, Department of Chemistry and Applied Biosciences, ETH Zürich, CH-8093 Zürich, Switzerland; Empa−Swiss Federal Laboratories for Materials Science and Technology, CH-8600 Dübendorf, Switzerland;* orcid.org/0000-0002-6409-0565

Federica Bertolotti − *Dipartimento di Scienza e Alta Tecnologia & To.Sca.Lab, Università dell'Insubria, 22100 Como, Italy;* orcid.org/0000-0002-6001-9040

Marcel Aebli − *Institute of Inorganic Chemistry, Department of Chemistry and Applied Biosciences, ETH Zürich, CH-8093 Zürich, Switzerland; Empa−Swiss Federal Laboratories for Materials Science and Technology, CH-8600 Dübendorf, Switzerland*

Richard D. Schaller − *Center for Nanoscale Materials, Argonne National Laboratory, Lemont, Illinois 60439, United States; Department of Chemistry, Northwestern University, Evanston, Illinois 60208, United States;* orcid.org/0000-0001-9696-8830

Alexander Wieczorek − *Empa−Swiss Federal Laboratories for Materials Science and Technology, CH-8600 Dübendorf, Switzerland;* orcid.org/0000-0002-1025-128X

Sebastian Siol − *Empa−Swiss Federal Laboratories for Materials Science and Technology, CH-8600 Dübendorf, Switzerland;* orcid.org/0000-0002-0907-6525

Claudia Cancellieri − *Empa−Swiss Federal Laboratories for Materials Science and Technology, CH-8600 Dübendorf, Switzerland;* orcid.org/0000-0003-4124-4362

Lars P. H. Jeurgens − *Empa−Swiss Federal Laboratories for Materials Science and Technology, CH-8600 Dübendorf, Switzerland;* orcid.org/0000-0002-0264-9220

Norberto Masciocchi − *Dipartimento di Scienza e Alta Tecnologia & To.Sca.Lab, Università dell'Insubria, 22100 Como, Italy;* orcid.org/0000-0001-9921-2350

Antonietta Guagliardi − *Istituto di Cristallografia & To.Sca.Lab, Consiglio Nazionale delle Ricerche, 22100 Como, Italy;* orcid.org/0000-0001-6390-2114

Laurent Pedesseau − *Univ Rennes, INSA Rennes, CNRS, Institut FOTON, Rennes F-35000, France;* orcid.org/0000-0001-9414-8644

Jacky Even − *Univ Rennes, INSA Rennes, CNRS, Institut FOTON, Rennes F-35000, France;* orcid.org/0000-0002-4607-3390

Maksym V. Kovalenko − *Institute of Inorganic Chemistry, Department of Chemistry and Applied Biosciences, ETH Zürich, CH-8093 Zürich, Switzerland; Empa−Swiss Federal Laboratories for Materials Science and Technology, CH-8600 Dübendorf, Switzerland;* orcid.org/0000-0002-6396-8938

Maryna I. Bodnarchuk − *Institute of Inorganic Chemistry, Department of Chemistry and Applied Biosciences, ETH Zürich, CH-8093 Zürich, Switzerland; Empa−Swiss Federal Laboratories for Materials Science and Technology, CH-8600 Dübendorf, Switzerland;* orcid.org/0000-0001-6597-3266

Complete contact information is available at: https://pubs.acs.org/10.1021/acs.nanolett.2c04927

Notes

The authors declare no competing financial interest.

■ ACKNOWLEDGMENTS

This project was supported by the European Union's Horizon 2020 research and innovation program under grant agreement No 862656 (project DROP-IT). This work was partially funded by the Swiss National Science Foundation (grant number 200021_192308, project Q-Light), the European Union through Horizon 2020 Research and Innovation Program (ERC CoG Grant, grant agreement number 819740, project SCALE-HALO), and MIUR (PRIN-2017L8WW48, Project HY-TEC). We acknowledge financial support from the Swiss National Science Foundation (R'Equip program, Proposal 206021_182987). A.W. acknowledges funding from the Strategic Focus Area−Advanced Manufacturing (SFA-AM) through the project Advancing manufacturability of hybrid organic−inorganic semiconductors for large area optoelectronics (AMYS). This work was performed, in part, at the Center for Nanoscale Materials, a U.S. Department of Energy Office of Science User Facility, and supported by the U.S. Department of Energy, Office of Science, under Contract No. DE-AC02-06CH11357. The authors acknowledge the support of the Electron Microscopy center at Empa, and scientific and technical staff of the MS-X04A beamline of the Swiss Light Source at Paul Scherrer Insitut (Villigen, CH). We acknowledge that the calculations of this research have been performed using the DECI resource Prometheus at CYFRONET in Poland (https://www.cyfronet.pl/) with support from the PRACE aisbl. The authors thank Dr. Martin Kotyrba for the help with the distillation in an ultrahigh vacuum and Prof. Christophe Coperet for providing Mashima's reagent.

■ REFERENCES

(1) Lee, M. M.; Teuscher, J.; Miyasaka, T.; Murakami, T. N.; Snaith, H. J. Efficient hybrid solar cells based on meso-superstructured organometal halide perovskites. *Science* **2012**, *338* (6107), 643−647.

(2) Burschka, J.; Pellet, N.; Moon, S.-J.; Humphry-Baker, R.; Gao, P.; Nazeeruddin, M. K.; Gratzel, M. Sequential deposition as a route to high-performance perovskite-sensitized solar cells. *Nature* **2013**, *499* (7458), 316−319.

(3) Dong, Q.; Fang, Y.; Shao, Y.; Mulligan, P.; Qiu, J.; Cao, L.; Huang, J. Electron-hole diffusion lengths > 175 μm in solution-grown $CH_3NH_3PbI_3$ single crystals. *Science* **2015**, *347* (6225), 967−970.

(4) Saidaminov, M. I.; Abdelhady, A. L.; Maculan, G.; Bakr, O. M. Retrograde solubility of formamidinium and methylammonium lead halide perovskites enabling rapid single crystal growth. *Chem. Commun.* **2015**, *51* (100), 17658−17661.

(5) Shi, D.; Adinolfi, V.; Comin, R.; Yuan, M.; Alarousu, E.; Buin, A.; Chen, Y.; Hoogland, S.; Rothenberger, A.; Katsiev, K.; Losovyj, Y.; Zhang, X.; Dowben, P. A.; Mohammed, O. F.; Sargent, E. H.; Bakr, O. M. Low trap-state density and long carrier diffusion in organolead trihalide perovskite single crystals. *Science* **2015**, *347* (6221), 519−522.

(6) Cao, Y.; Wang, N.; Tian, H.; Guo, J.; Wei, Y.; Chen, H.; Miao, Y.; Zou, W.; Pan, K.; He, Y.; Cao, H.; Ke, Y.; Xu, M.; Wang, Y.; Yang, M.; Du, K.; Fu, Z.; Kong, D.; Dai, D.; Jin, Y.; Li, G.; Li, H.; Peng, Q.; Wang, J.; Huang, W. Perovskite light-emitting diodes based on spontaneously formed submicrometre-scale structures. *Nature* **2018**, *562* (7726), 249−253.

(7) Lin, K.; Xing, J.; Quan, L. N.; de Arquer, F. P. G.; Gong, X.; Lu, J.; Xie, L.; Zhao, W.; Zhang, D.; Yan, C.; Li, W.; Liu, X.; Lu, Y.; Kirman, J.; Sargent, E. H.; Xiong, Q.; Wei, Z. Perovskite light-emitting diodes with external quantum efficiency exceeding 20%. *Nature* **2018**, *562* (7726), 245−248.

(8) Wang, J.; Song, C.; He, Z.; Mai, C.; Xie, G.; Mu, L.; Cun, Y.; Li, J.; Wang, J.; Peng, J.; Cao, Y. All-Solution-Processed Pure Formamidinium-Based Perovskite Light-Emitting Diodes. *Adv. Mater.* **2018**, *30* (39), 1804137.

(9) Hassan, Y.; Park, J. H.; Crawford, M. L.; Sadhanala, A.; Lee, J.; Sadighian, J. C.; Mosconi, E.; Shivanna, R.; Radicchi, E.; Jeong, M.; Yang, C.; Choi, H.; Park, S. H.; Song, M. H.; De Angelis, F.; Wong, C. Y.; Friend, R. H.; Lee, B. R.; Snaith, H. J. Ligand-engineered bandgap stability in mixed-halide perovskite LEDs. *Nature* **2021**, *591* (7848), 72−77.

(10) Xue, J.; Zhu, Z.; Xu, X.; Gu, Y.; Wang, S.; Xu, L.; Zou, Y.; Song, J.; Zeng, H.; Chen, Q. Narrowband Perovskite Photodetector-Based Image Array for Potential Application in Artificial Vision. *Nano Lett.* **2018**, *18* (12), 7628−7634.

(11) Chen, Q.; Wu, J.; Ou, X.; Huang, B.; Almutlaq, J.; Zhumekenov, A. A.; Guan, X.; Han, S.; Liang, L.; Yi, Z.; Li, J.; Xie, X.; Wang, Y.; Li, Y.; Fan, D.; Teh, D. B. L.; All, A. H.; Mohammed, O. F.; Bakr, O. M.; Wu, T.; Bettinelli, M.; Yang, H.; Huang, W.; Liu, X. All-inorganic perovskite nanocrystal scintillators. *Nature* **2018**, *561* (7721), 88−93.

(12) Heo, J. H.; Shin, D. H.; Park, J. K.; Kim, D. H.; Lee, S. J.; Im, S. H. High-Performance Next-Generation Perovskite Nanocrystal Scintillator for Nondestructive X-Ray Imaging. *Adv. Mater.* **2018**, *30* (40), 1801743.

(13) Yakunin, S.; Dirin, D. N.; Shynkarenko, Y.; Morad, V.; Cherniukh, I.; Nazarenko, O.; Kreil, D.; Nauser, T.; Kovalenko, M. V. Detection of gamma photons using solution-grown single crystals of hybrid lead halide perovskites. *Nat. Photon* **2016**, *10* (9), 585−589.

(14) Yakunin, S.; Sytnyk, M.; Kriegner, D.; Shrestha, S.; Richter, M.; Matt, G. J.; Azimi, H.; Brabec, C. J.; Stangl, J.; Kovalenko, M. V.; Heiss, W. Detection of X-ray photons by solution-processed lead halide perovskites. *Nat. Photon* **2015**, *9* (7), 444−449.

(15) McCall, K. M.; Sakhatskyi, K.; Lehmann, E.; Walfort, B.; Losko, A. S.; Montanarella, F.; Bodnarchuk, M. I.; Krieg, F.; Kelestemur, Y.; Mannes, D.; Shynkarenko, Y.; Yakunin, S.; Kovalenko, M. V. Fast Neutron Imaging with Semiconductor Nanocrystal Scintillators. *ACS Nano* **2020**, *14* (11), 14686−14697.

(16) Fang, H.-H.; Adjokatse, S.; Wei, H.; Yang, J.; Blake, G. R.; Huang, J.; Even, J.; Loi, M. A. Ultrahigh sensitivity of methylammonium lead tribromide perovskite single crystals to environmental gases. *Science Advances* **2016**, *2* (7), No. e1600534.

(17) Manser, J. S.; Christians, J. A.; Kamat, P. V. Intriguing Optoelectronic Properties of Metal Halide Perovskites. *Chem. Rev.* **2016**, *116*, 12956−13008.
(18) Maculan, G.; Sheikh, A. D.; Abdelhady, A. L.; Saidaminov, M. I.; Haque, M. A.; Murali, B.; Alarousu, E.; Mohammed, O. F.; Wu, T.; Bakr, O. M. $CH_3NH_3PbCl_3$ Single Crystals: Inverse Temperature Crystallization and Visible-Blind UV-Photodetector. *J. Phys. Chem. Lett.* **2015**, *6* (19), 3781−3786.
(19) Saidaminov, M. I.; Abdelhady, A. L.; Murali, B.; Alarousu, E.; Burlakov, V. M.; Peng, W.; Dursun, I.; Wang, L.; He, Y.; Maculan, G.; Goriely, A.; Wu, T.; Mohammed, O. F.; Bakr, O. M. High-quality bulk hybrid perovskite single crystals within minutes by inverse temperature crystallization. *Nat. Commun.* **2015**, *6*, 7586.
(20) Stoumpos, C. C.; Malliakas, C. D.; Peters, J. A.; Liu, Z.; Sebastian, M.; Im, J.; Chasapis, T. C.; Wibowo, A. C.; Chung, D. Y.; Freeman, A. J.; Wessels, B. W.; Kanatzidis, M. G. Crystal Growth of the Perovskite Semiconductor $CsPbBr_3$: A New Material for High-Energy Radiation Detection. *Cryst. Growth Des.* **2013**, *13* (7), 2722−2727.
(21) Lian, Z.; Yan, Q.; Gao, T.; Ding, J.; Lv, Q.; Ning, C.; Li, Q.; Sun, J.-l. Perovskite $CH_3NH_3PbI_3(Cl)$ Single Crystals: Rapid Solution Growth, Unparalleled Crystalline Quality, and Low Trap Density toward 108 cm^{-3}. *J. Am. Chem. Soc.* **2016**, *138* (30), 9409−9412.
(22) Zhu, H.; Trinh, M. T.; Wang, J.; Fu, Y.; Joshi, P. P.; Miyata, K.; Jin, S.; Zhu, X.-Y. Organic Cations Might Not Be Essential to the Remarkable Properties of Band Edge Carriers in Lead Halide Perovskites. *Adv. Mater.* **2017**, *29* (1), 1603072.
(23) Zhu, H.; Miyata, K.; Fu, Y.; Wang, J.; Joshi Prakriti, P.; Niesner, D.; Williams Kristopher, W.; Jin, S.; Zhu, X. Y. Screening in crystalline liquids protects energetic carriers in hybrid perovskites. *Science* **2016**, *353* (6306), 1409−1413.
(24) Miyata, A.; Mitioglu, A.; Plochocka, P.; Portugall, O.; Wang, J. T.-W.; Stranks, S. D.; Snaith, H. J.; Nicholas, R. J. Direct measurement of the exciton binding energy and effective masses for charge carriers in organic-inorganic tri-halide perovskites. *Nat. Phys.* **2015**, *11* (7), 582−587.
(25) Kovalenko, M. V.; Protesescu, L.; Bodnarchuk, M. I. Properties and potential optoelectronic applications of lead halide perovskite nanocrystals. *Science* **2017**, *358* (6364), 745−750.
(26) Dirin, D. N.; Benin, B. M.; Yakunin, S.; Krumeich, F.; Raino, G.; Frison, R.; Kovalenko, M. V. Microcarrier-Assisted Inorganic Shelling of Lead Halide Perovskite Nanocrystals. *ACS Nano* **2019**, *13* (10), 11642−11652.
(27) Babayigit, A.; Ethirajan, A.; Muller, M.; Conings, B. Toxicity of organometal halide perovskite solar cells. *Nat. Mater.* **2016**, *15* (3), 247−251.
(28) Brandt, R. E.; Stevanović, V.; Ginley, D. S.; Buonassisi, T. Identifying defect-tolerant semiconductors with high minority-carrier lifetimes: beyond hybrid lead halide perovskites. *MRS Commun.* **2015**, *5* (02), 265−275.
(29) Dirin, D. N.; Protesescu, L.; Trummer, D.; Kochetygov, I. V.; Yakunin, S.; Krumeich, F.; Stadie, N. P.; Kovalenko, M. V. Harnessing Defect-Tolerance at the Nanoscale: Highly Luminescent Lead Halide Perovskite Nanocrystals in Mesoporous Silica Matrixes. *Nano Lett.* **2016**, *16* (9), 5866−5874.
(30) Zhu, X. Y.; Podzorov, V. Charge Carriers in Hybrid Organic−Inorganic Lead Halide Perovskites Might Be Protected as Large Polarons. *J. Phys. Chem. Lett.* **2015**, *6* (23), 4758−4761.
(31) Miyata, K.; Meggiolaro, D.; Trinh, M. T.; Joshi Prakriti, P.; Mosconi, E.; Jones Skyler, C.; De Angelis, F.; Zhu, X. Y. Large polarons in lead halide perovskites. *Sci. Adv.* **2017**, *3* (8), e1701217.
(32) Puppin, M.; Polishchuk, S.; Colonna, N.; Crepaldi, A.; Dirin, D. N.; Nazarenko, O.; De Gennaro, R.; Gatti, G.; Roth, S.; Barillot, T.; Poletto, L.; Xian, R. P.; Rettig, L.; Wolf, M.; Ernstorfer, R.; Kovalenko, M. V.; Marzari, N.; Grioni, M.; Chergui, M. Evidence of Large Polarons in Photoemission Band Mapping of the Perovskite SemiconductorCsPbBr$_3$. *Phys. Rev. Lett.* **2020**, *124* (20), 206402.
(33) Ghosh, D.; Welch, E.; Neukirch, A. J.; Zakhidov, A.; Tretiak, S. Polarons in Halide Perovskites: A Perspective. *J. Phys. Chem. Lett.* **2020**, *11* (9), 3271−3286.
(34) Stoumpos, C. C.; Kanatzidis, M. G. The Renaissance of Halide Perovskites and Their Evolution as Emerging Semiconductors. *Acc. Chem. Res.* **2015**, *48* (10), 2791−2802.
(35) Infante, I.; Manna, L. Are There Good Alternatives to Lead Halide Perovskite Nanocrystals? *Nano Lett.* **2021**, *21* (1), 6−9.
(36) McCall, K. M.; Morad, V.; Benin, B. M.; Kovalenko, M. V. Efficient Lone-Pair-Driven Luminescence: Structure−Property Relationships in Emissive $5s^2$ Metal Halides. *ACS Materials Letters* **2020**, *2* (9), 1218−1232.
(37) Noculak, A.; Morad, V.; McCall, K. M.; Yakunin, S.; Shynkarenko, Y.; Wörle, M.; Kovalenko, M. V. Bright Blue and Green Luminescence of Sb(III) in Double Perovskite Cs_2MInCl_6 (M = Na, K) Matrices. *Chem. Mater.* **2020**, *32* (12), 5118−5124.
(38) Khalfin, S.; Bekenstein, Y. Advances in lead-free double perovskite nanocrystals, engineering band-gaps and enhancing stability through composition tunability. *Nanoscale* **2019**, *11* (18), 8665−8679.
(39) Zhou, C.; Lin, H.; He, Q.; Xu, L.; Worku, M.; Chaaban, M.; Lee, S.; Shi, X.; Du, M.-H.; Ma, B. Low dimensional metal halide perovskites and hybrids. *Materials Science and Engineering: R: Reports* **2019**, *137*, 38−65.
(40) Xuan, T.; Xie, R.-J. Recent processes on light-emitting lead-free metal halide perovskites. *Chemical Engineering Journal* **2020**, *393*, 124757.
(41) Slavney, A. H.; Hu, T.; Lindenberg, A. M.; Karunadasa, H. I. A Bismuth-Halide Double Perovskite with Long Carrier Recombination Lifetime for Photovoltaic Applications. *J. Am. Chem. Soc.* **2016**, *138* (7), 2138−2141.
(42) Jodlowski, A.; Rodríguez-Padrón, D.; Luque, R.; de Miguel, G. Alternative Perovskites for Photovoltaics. *Adv. Energy Mater.* **2018**, *8* (21), 1703120.
(43) Igbari, F.; Wang, Z.-K.; Liao, L.-S. Progress of Lead-Free Halide Double Perovskites. *Adv. Energy Mater.* **2019**, *9* (12), 1803150.
(44) Yang, J.; Bao, C.; Ning, W.; Wu, B.; Ji, F.; Yan, Z.; Tao, Y.; Liu, J.-M.; Sum, T. C.; Bai, S.; Wang, J.; Huang, W.; Zhang, W.; Gao, F. Stable, High-Sensitivity and Fast-Response Photodetectors Based on Lead-Free $Cs_2AgBiBr_6$ Double Perovskite Films. *Advanced Optical Materials* **2019**, *7* (13), 1801732.
(45) Yakunin, S.; Benin, B. M.; Shynkarenko, Y.; Nazarenko, O.; Bodnarchuk, M. I.; Dirin, D. N.; Hofer, C.; Cattaneo, S.; Kovalenko, M. V. High-resolution remote thermometry and thermography using luminescent low-dimensional tin-halide perovskites. *Nat. Mater.* **2019**, *18* (8), 846−852.
(46) Zhang, X.; Wang, C.; Zhang, Y.; Zhang, X.; Wang, S.; Lu, M.; Cui, H.; Kershaw, S. V.; Yu, W. W.; Rogach, A. L. Bright Orange Electroluminescence from Lead-Free Two-Dimensional Perovskites. *ACS Energy Letters* **2019**, *4* (1), 242−248.
(47) Maughan, A. E.; Ganose, A. M.; Bordelon, M. M.; Miller, E. M.; Scanlon, D. O.; Neilson, J. R. Defect Tolerance to Intolerance in the Vacancy-Ordered Double Perovskite Semiconductors Cs_2SnI_6 and Cs_2TeI_6. *J. Am. Chem. Soc.* **2016**, *138* (27), 8453−8464.
(48) Gupta, S.; Cahen, D.; Hodes, G. How SnF_2 Impacts the Material Properties of Lead-Free Tin Perovskites. *J. Phys. Chem. C* **2018**, *122* (25), 13926−13936.
(49) Nishimura, K.; Kamarudin, M. A.; Hirotani, D.; Hamada, K.; Shen, Q.; Iikubo, S.; Minemoto, T.; Yoshino, K.; Hayase, S. Lead-free tin-halide perovskite solar cells with 13% efficiency. *Nano Energy* **2020**, *74*, 104858.
(50) Zhu, Z.; Jiang, X.; Yu, D.; Yu, N.; Ning, Z.; Mi, Q. Smooth and Compact FASnI3 Films for Lead-Free Perovskite Solar Cells with over 14% Efficiency. *ACS Energy Letters* **2022**, *7* (6), 2079−2083.
(51) Lin, R.; Xiao, K.; Qin, Z.; Han, Q.; Zhang, C.; Wei, M.; Saidaminov, M. I.; Gao, Y.; Xu, J.; Xiao, M.; Li, A.; Zhu, J.; Sargent, E. H.; Tan, H. Monolithic all-perovskite tandem solar cells with 24.8% efficiency exploiting comproportionation to suppress Sn(ii) oxidation in precursor ink. *Nature Energy* **2019**, *4* (10), 864−873.

https://doi.org/10.1021/acs.nanolett.2c04927
Nano Lett. 2023, 23, 1914−1923

(52) Nakamura, T.; Yakumaru, S.; Truong, M. A.; Kim, K.; Liu, J.; Hu, S.; Otsuka, K.; Hashimoto, R.; Murdey, R.; Sasamori, T.; Kim, H. D.; Ohkita, H.; Handa, T.; Kanemitsu, Y.; Wakamiya, A. Sn(IV)-free tin perovskite films realized by in situ Sn(0) nanoparticle treatment of the precursor solution. *Nat. Commun.* **2020**, *11* (1), 3008.
(53) Ke, W.; Stoumpos Constantinos, C.; Zhu, M.; Mao, L.; Spanopoulos, I.; Liu, J.; Kontsevoi Oleg, Y.; Chen, M.; Sarma, D.; Zhang, Y.; Wasielewski Michael, R.; Kanatzidis Mercouri, G. Enhanced photovoltaic performance and stability with a new type of hollow 3D perovskite {en}FASnI$_3$. *Sci. Adv.* **2017**, *3* (8), No. e1701293.
(54) Ke, W.; Stoumpos, C. C.; Spanopoulos, I.; Chen, M.; Wasielewski, M. R.; Kanatzidis, M. G. Diammonium Cations in the FASnI$_3$ Perovskite Structure Lead to Lower Dark Currents and More Efficient Solar Cells. *ACS Energy Letters* **2018**, *3* (7), 1470−1476.
(55) Jokar, E.; Chien, C.-H.; Fathi, A.; Rameez, M.; Chang, Y.-H.; Diau, E. W.-G. Slow surface passivation and crystal relaxation with additives to improve device performance and durability for tin-based perovskite solar cells. *Energy Environ. Sci.* **2018**, *11* (9), 2353−2362.
(56) Spanopoulos, I.; Ke, W.; Stoumpos, C. C.; Schueller, E. C.; Kontsevoi, O. Y.; Seshadri, R.; Kanatzidis, M. G. Unraveling the Chemical Nature of the 3D "Hollow" Hybrid Halide Perovskites. *J. Am. Chem. Soc.* **2018**, *140* (17), 5728−5742.
(57) Tsai, C.-M.; Lin, Y.-P.; Pola, M. K.; Narra, S.; Jokar, E.; Yang, Y.-W.; Diau, E. W.-G. Control of Crystal Structures and Optical Properties with Hybrid Formamidinium and 2-Hydroxyethylammonium Cations for Mesoscopic Carbon-Electrode Tin-Based Perovskite Solar Cells. *ACS Energy Letters* **2018**, *3* (9), 2077−2085.
(58) Jokar, E.; Chien, C.-H.; Tsai, C.-M.; Fathi, A.; Diau, E. W.-G. Robust Tin-Based Perovskite Solar Cells with Hybrid Organic Cations to Attain Efficiency Approaching 10%. *Adv. Mater.* **2019**, *31* (2), 1804835.
(59) Gao, W.; Chen, C.; Ran, C.; Zheng, H.; Dong, H.; Xia, Y.; Chen, Y.; Huang, W. A-Site Cation Engineering of Metal Halide Perovskites: Version 3.0 of Efficient Tin-Based Lead-Free Perovskite Solar Cells. *Adv. Funct. Mater.* **2020**, *30* (34), 2000794.
(60) Naumkin, A. V. K.-V. A.; Gaarenstroom, S. W.; Powell, C. J. *NIST X-ray Photoelectron Spectroscopy Database*, Version 4.1. http://srdata.nist.gov/xps/ (accessed on 03-02-2023).
(61) Chen, L.-J.; Lee, C.-R.; Chuang, Y.-J.; Wu, Z.-H.; Chen, C. Synthesis and Optical Properties of Lead-Free Cesium Tin Halide Perovskite Quantum Rods with High-Performance Solar Cell Application. *J. Phys. Chem. Lett.* **2016**, *7* (24), 5028−5035.
(62) Jellicoe, T. C.; Richter, J. M.; Glass, H. F. J.; Tabachnyk, M.; Brady, R.; Dutton, S. E.; Rao, A.; Friend, R. H.; Credgington, D.; Greenham, N. C.; Böhm, M. L. Synthesis and Optical Properties of Lead-Free Cesium Tin Halide Perovskite Nanocrystals. *J. Am. Chem. Soc.* **2016**, *138* (9), 2941−2944.
(63) Wong, A. B.; Bekenstein, Y.; Kang, J.; Kley, C. S.; Kim, D.; Gibson, N. A.; Zhang, D.; Yu, Y.; Leone, S. R.; Wang, L.-W.; Alivisatos, A. P.; Yang, P. Strongly Quantum Confined Colloidal Cesium Tin Iodide Perovskite Nanoplates: Lessons for Reducing Defect Density and Improving Stability. *Nano Lett.* **2018**, *18* (3), 2060−2066.
(64) Lin, C.; Chen, D.; Weng, K.; Jiao, Q.; Ren, J.; Dai, S. Glassy Flux Protocol to Confine Lead-Free CsSnX$_3$ Nanocrystals into Transparent Solid Medium. *J. Phys. Chem. Lett.* **2020**, *11* (15), 6084−6089.
(65) Liu, Q.; Yin, J.; Zhang, B.-B.; Chen, J.-K.; Zhou, Y.; Zhang, L.-M.; Wang, L.-M.; Zhao, Q.; Hou, J.; Shu, J.; Song, B.; Shirahata, N.; Bakr, O. M.; Mohammed, O. F.; Sun, H.-T. Theory-Guided Synthesis of Highly Luminescent Colloidal Cesium Tin Halide Perovskite Nanocrystals. *J. Am. Chem. Soc.* **2021**, *143* (14), 5470−5480.
(66) Bhaumik, S.; Ray, S.; Batabyal, S. K. Recent advances of lead-free metal halide perovskite single crystals and nanocrystals: synthesis, crystal structure, optical properties, and their diverse applications. *Materials Today Chemistry* **2020**, *18*, 100363.
(67) Swarnkar, A.; Ravi, V. K.; Nag, A. Beyond Colloidal Cesium Lead Halide Perovskite Nanocrystals: Analogous Metal Halides and Doping. *ACS Energy Letters* **2017**, *2* (5), 1089−1098.
(68) Gahlot, K.; de Graaf, S.; Duim, H.; Nedelcu, G.; Koushki, R. M.; Ahmadi, M.; Gavhane, D.; Lasorsa, A.; De Luca, O.; Rudolf, P.; van der Wel, P. C. A.; Loi, M. A.; Kooi, B. J.; Portale, G.; Calbo, J.; Protesescu, L. Structural Dynamics and Tunability for Colloidal Tin Halide Perovskite Nanostructures. *Adv. Mater.* **2022**, *34* (30), 2201353.
(69) Chen, Y.; Yin, J.; Wei, Q.; Wang, C.; Wang, X.; Ren, H.; Yu, S. F.; Bakr, O. M.; Mohammed, O. F.; Li, M. Multiple exciton generation in tin−lead halide perovskite nanocrystals for photocurrent quantum efficiency enhancement. *Nat. Photonics* **2022**, *16* (7), 485−490.
(70) Dai, L.; Deng, Z.; Auras, F.; Goodwin, H.; Zhang, Z.; Walmsley, J. C.; Bristowe, P. D.; Deschler, F.; Greenham, N. C. Slow carrier relaxation in tin-based perovskite nanocrystals. *Nat. Photonics* **2021**, *15* (9), 696−702.
(71) Wieczorek, A.; Lai, H.; Pious, J.; Fu, F.; Siol, S. Resolving Oxidation States and X−site Composition of Sn Perovskites through Auger Parameter Analysis in XPS. *Adv. Mater. Interfaces* **2022**, 2201828.
(72) Gaarenstroom, S. W.; Winograd, N. Initial and final state effects in the ESCA spectra of cadmium and silver oxides. *J. Chem. Phys.* **1977**, *67* (8), 3500−3506.
(73) Jeurgens, L. P. H.; Reichel, F.; Frank, S.; Richter, G.; Mittemeijer, E. J. On the development of long-range order in ultra-thin amorphous Al2O3 films upon their transformation into crystalline γ-Al2O3. *Surf. Interface Anal.* **2008**, *40* (3−4), 259−263.
(74) Zhuk, S.; Siol, S. Chemical state analysis of reactively sputtered zinc vanadium nitride: The Auger parameter as a tool in materials design. *Appl. Surf. Sci.* **2022**, *601*, 154172.
(75) Kubicki, D. J.; Prochowicz, D.; Salager, E.; Rakhmatullin, A.; Grey, C. P.; Emsley, L.; Stranks, S. D. Local Structure and Dynamics in Methylammonium, Formamidinium, and Cesium Tin(II) Mixed-Halide Perovskites from ^{119}Sn Solid-State NMR. *J. Am. Chem. Soc.* **2020**, *142* (17), 7813−7826.
(76) Siol, S.; Mann, J.; Newman, J.; Miyayama, T.; Watanabe, K.; Schmutz, P.; Cancellieri, C.; Jeurgens, L. P. H. Concepts for chemical state analysis at constant probing depth by lab-based XPS/HAXPES combining soft and hard X-ray sources. *Surf. Interface Anal.* **2020**, *52* (12), 802−810.
(77) Tan, Y.; Zou, Y.; Wu, L.; Huang, Q.; Yang, D.; Chen, M.; Ban, M.; Wu, C.; Wu, T.; Bai, S.; Song, T.; Zhang, Q.; Sun, B. Highly Luminescent and Stable Perovskite Nanocrystals with Octylphosphonic Acid as a Ligand for Efficient Light-Emitting Diodes. *ACS Appl. Mater. Interfaces* **2018**, *10* (4), 3784−3792.
(78) Fang, H.-H.; Adjokatse, S.; Shao, S.; Even, J.; Loi, M. A. Long-lived hot-carrier light emission and large blue shift in formamidinium tin triiodide perovskites. *Nat. Commun.* **2018**, *9* (1), 243.
(79) Protesescu, L.; Yakunin, S.; Kumar, S.; Bär, J.; Bertolotti, F.; Masciocchi, N.; Guagliardi, A.; Grotevent, M.; Shorubalko, I.; Bodnarchuk, M. I.; Shih, C.-J.; Kovalenko, M. V. Dismantling the "Red Wall" of Colloidal Perovskites: Highly Luminescent Formamidinium and Formamidinium−Cesium Lead Iodide Nanocrystals. *ACS Nano* **2017**, *11* (3), 3119−3134.
(80) Zhao, Q.; Hazarika, A.; Schelhas, L. T.; Liu, J.; Gaulding, E. A.; Li, G.; Zhang, M.; Toney, M. F.; Sercel, P. C.; Luther, J. M. Size-Dependent Lattice Structure and Confinement Properties in CsPbI$_3$ Perovskite Nanocrystals: Negative Surface Energy for Stabilization. *ACS Energy Letters* **2020**, *5* (1), 238−247.
(81) Filippetti, A.; Kahmann, S.; Caddeo, C.; Mattoni, A.; Saba, M.; Bosin, A.; Loi, M. A. Fundamentals of tin iodide perovskites: a promising route to highly efficient, lead-free solar cells. *Journal of Materials Chemistry A* **2021**, *9* (19), 11812−11826.
(82) Roknuzzaman, M.; Alarco, J. A.; Wang, H.; Du, A.; Tesfamichael, T.; Ostrikov, K. Ab initio atomistic insights into lead-free formamidinium based hybrid perovskites for photovoltaics and optoelectronics. *Comput. Mater. Sci.* **2019**, *169*, 109118.

(83) Ghimire, K.; Zhao, D.; Yan, Y.; Podraza, N. J. Optical response of mixed methylammonium lead iodide and formamidinium tin iodide perovskite thin films. *AIP Advances* **2017**, *7* (7), No. 075108.
(84) Li, Y.; Luo, X.; Liu, Y.; Lu, X.; Wu, K. Size- and Composition-Dependent Exciton Spin Relaxation in Lead Halide Perovskite Quantum Dots. *ACS Energy Letters* **2020**, *5* (5), 1701−1708.
(85) Liang, W.; Li, Y.; Xiang, D.; Han, Y.; Jiang, Q.; Zhang, W.; Wu, K. Efficient Optical Orientation and Slow Spin Relaxation in Lead-Free $CsSnBr_3$ Perovskite Nanocrystals. *ACS Energy Letters* **2021**, *6* (5), 1670−1676.
(86) Ouhbi, H.; Ambrosio, F.; De Angelis, F.; Wiktor, J. Strong Electron Localization in Tin Halide Perovskites. *J. Phys. Chem. Lett.* **2021**, *12* (22), 5339−5343.
(87) Kahmann, S.; Nazarenko, O.; Shao, S.; Hordiichuk, O.; Kepenekian, M.; Even, J.; Kovalenko, M. V.; Blake, G. R.; Loi, M. A. Negative Thermal Quenching in $FASnI_3$ Perovskite Single Crystals and Thin Films. *ACS Energy Letters* **2020**, *5* (8), 2512−2519.
(88) Schueller, E. C.; Laurita, G.; Fabini, D. H.; Stoumpos, C. C.; Kanatzidis, M. G.; Seshadri, R. Crystal Structure Evolution and Notable Thermal Expansion in Hybrid Perovskites Formamidinium Tin Iodide and Formamidinium Lead Bromide. *Inorg. Chem.* **2018**, *57* (2), 695−701.
(89) Paufler, P. *The Rietveld Method. International Union of Crystallography.*; John Wiley & Sons, Ltd, 1995; Vol. *30*, p 298.
(90) Debye, P. Zerstreuung von Röntgenstrahlen. *Annalen der Physik* **1915**, *351* (6), 809−823.
(91) Protesescu, L.; Yakunin, S.; Bodnarchuk, M. I.; Bertolotti, F.; Masciocchi, N.; Guagliardi, A.; Kovalenko, M. V. Monodisperse Formamidinium Lead Bromide Nanocrystals with Bright and Stable Green Photoluminescence. *J. Am. Chem. Soc.* **2016**, *138* (43), 14202−14205.
(92) Laurita, G.; Fabini, D. H.; Stoumpos, C. C.; Kanatzidis, M. G.; Seshadri, R. Chemical tuning of dynamic cation off-centering in the cubic phases of hybrid tin and lead halide perovskites. *Chemical Science* **2017**, *8* (8), 5628−5635.
(93) Zacharias, M.; Giustino, F. Theory of the special displacement method for electronic structure calculations at finite temperature. *Physical Review Research* **2020**, *2* (1), No. 013357.
(94) Quarti, C.; Mosconi, E.; Ball, J. M.; D'Innocenzo, V.; Tao, C.; Pathak, S.; Snaith, H. J.; Petrozza, A.; De Angelis, F. Structural and optical properties of methylammonium lead iodide across the tetragonal to cubic phase transition: implications for perovskite solar cells. *Energy Environ. Sci.* **2016**, *9* (1), 155−163.

https://doi.org/10.1021/acs.nanolett.2c04927
Nano Lett. 2023, 23, 1914−1923